Available online at www.sciencedirect.com
SCIENCE DIRECT®
Polymer 44 (2003) 8119–8132
polymer
www.elsevier.com/locate/polymer

Crystallization kinetics and melting behaviors of nylon 6/foliated graphite nanocomposites

Wengui Weng, Guohua Chen*, Dajun Wu

College of Materials Science and Engineering, Huaqiao University, Quanzhou 362011, People's Republic of China

Received 25 May 2003; received in revised form 8 October 2003; accepted 14 October 2003

Abstract

This article studies the crystallization kinetics and melting behaviors of nylon 6/foliated graphite electrically conducting nanocomposites. The crystallization kinetics under isothermal conditions is described by the Avrami equation. The values of the exponent found for the neat nylon 6 and the nanocomposite samples are about 3.0 and 1.2, respectively. For non-isothermal studies, the Avrami equation modified by Jeziorny, the Ozawa theory, the modified Ozawa equation and an equation combining the Avrami and Ozawa equation are employed. It is found that the Ozawa analysis fails to provide an adequate description of the non-isothermal crystallization process in both the neat nylon 6 and the nanocomposite samples. While the combination of Avrami and Ozawa equations exhibit great advantages in treating the non-isothermal crystallization kinetics. The activation energies are also determined by the Arrhenius relation and the Kissinger method for isothermal and non-isothermal crystallization, respectively. In both cases, the activation energy for the nanocomposite sample is greater than that for the neat nylon 6. In addition, subsequent DSC scans have also been performed to investigate the melting behaviors of the isothermally and non-isothermally crystallized samples. Results reveal that the isothermally crystallized samples exhibit two melting endotherms, while only the neat nylon 6 sample shows two melting endotherms after non-isothermal crystallization. The equilibrium melting temperature obtained is lower for the nanocomposite sample than for the neat nylon 6.

Keywords: Nylon 6; Foliated graphite; Nanocomposite

1. Introduction

Recently, fabrication of polymer/graphite conducting nanocomposites in the presence of expanded graphite (EG) particles has gained much attention since in these situations only a little amount of the conductive filler was needed to reach the percolation threshold of conductivity [1–6]. However, we [2–4] have shown that because of the interconnection of graphite subparticles in the worm-like expanded graphite, effective dispersion of the graphite nanosheets could hardly be achieved. Thus, a simple but effective procedure was developed to prepare separate graphite nanosheets from EG. The resulting foliated graphite nanosheets have been successfully incorporated into PMMA [7] and PS [8], and only about 1.0 wt% of the foliated graphite was required to satisfy the critical transition in both cases. In a proceeding work [9], with the assistance of ultrasonic irradiation we have also in situ synthesized nylon 6/FG nanocomposites, which exhibited a percolation threshold of as low as ca. 0.74 vol%. Now that the mechanisms [9] determining the extremely low percolation threshold and the electrical transport properties of the nanocomposites [10,11] have been well studied, we would like to further our studies on the crystallization and melting behaviors of the nylon 6/FG nanocomposites.

It is well understood that the physical, chemical and mechanical properties of crystalline polymers depend on the morphology, the crystalline structure and degree of crystallization. In order to control the rate of the crystallization and the degree of crystallinity and to obtain the desired morphology and properties, a great deal of effort has been devoted into studying the crystallization kinetics and determining the change in material properties [12,13]. While there have been a few papers [13–15] dealing with the crystallization behavior of neat nylon 6 and nylon 6/clay nanocomposites, little work has been done on graphite filled nylon 6 composites.

In practical processing, crystallization usually proceeds

* Corresponding author. Tel.: +86-5952692956; fax: +86-5952686969.
E-mail address: hdcgh@hqu.edu.cn (G. Chen). Contract grant sponsor: National Natural Foundation of China, No. 20174012.

0032-3861/$ - see front matter © 2003 Elsevier Ltd. All rights reserved.
doi:10.1016/j.polymer.2003.10.028

under isothermal and non-isothermal conditions. Therefore, it is important to investigate both the quiescent and dynamic crystallization kinetics of the polymer. In this work, the studies of isothermal and non-isothermal crystallization kinetics and melting behaviors of the nylon 6/foliated graphite nanocomposites were carried out by differential scanning calorimetry (DSC). The activation energies for isothermal and non-isothermal crystallization have also been evaluated.

2. Experimental

2.1. Materials and preparation

Detailed procedures for preparation of nylon 6/FG nanocomposites have been described in the proceeding paper [9]. Briefly, the desired volume content, ϕ, of the foliated graphite particles with an average thickness of about 50 nm and an average diameter of about 12 μm was incorporated into the molten ϵ-Caprolactam monomer. After homogenization of the molten monomer and FG mixture by ultrasonic irradiation, polymerization of the monomer was carried out using sodium hydroxide as activator and toluyl diisocyanate as chain initiator. This protocol used led to samples of various concentrations in conducting charge. The nylon 6/FG obtained containing 0.00 wt% (neat or pure nylon 6) and 1.50 wt% foliated graphite were used in this study.

2.2. Differential scanning calorimetry procedures

Perkin–Elmer DSC-7 and TA 2910 differential scanning calorimeters were used to analyze the isothermal and non-isothermal crystallization and subsequent melting behaviors, respectively. The temperature scale of the DSC was calibrated from the melting point (429.78) of high purity (99.999%) indium metal. The power response of the calorimeter was calibrated from the enthalpy of fusion of indium [12], taken to be 28.47 J/g. Samples of about 10 mg were accurately weighted, then placed in the DSC cell. All DSC analyses were performed under nitrogen atmosphere.

The isothermal crystallization and melting process of nylon 6 composite samples were performed as follows: the samples were heated at 100 °C/min to 250 °C and melt there for 5 min to eliminate any previous thermal history; then they were cooled at −150 °C/min to the predetermined crystallization temperature, T_c, in the range 188–194 °C in steps of 2 °C, and maintained at T_c for 20 min necessary for DSC trace return to the calorimeter baseline. The exothermal curves of heat flow as a function of time were recorded. Then the samples were quickly cooled at a cooling rate of −150 °C/min to 50 °C, maintained at this temperature for 5 min, and heated to 250 °C at a rate of 20 °C/min. The endothermal curves were also recorded to analyze the melting behaviors.

The non-isothermal crystallization and melting process of nylon 6 samples were performed as follows: the samples were heated from 25 to 250 °C, about 20 °C above the melting temperature of nylon 6, at a rate of 100 °C/min. The samples were kept for 5 min at this temperature to eliminate the heat history before cooling at a specified cooling rate. The samples were then cooled to 50 °C at constant cooling rate of 5, 10, 15, 20 °C/min. After keeping at 50 °C for 5 min, samples were heated to 250 °C at a heating rate of 20 °C/min, followed by the next cooling and heating cycle. Both the exothermic an endothermic curves were recorded.

3. Results and discussion

3.1. Isothermal crystallization analysis

3.1.1. Analysis based on the Avrami equation

The isothermal crystallization exotherms of pure nylon 6 and nylon 6/FG nanocomposite with a foliated graphite weight content of 1.50%, obtained as described in Section 2, are shown in Fig. 1. It is seen that for both of the two samples, the crystallization exothermic peak becomes flatter, and the time to reach the maximum degree of crystallization increases, as the increase of the crystallization temperature.

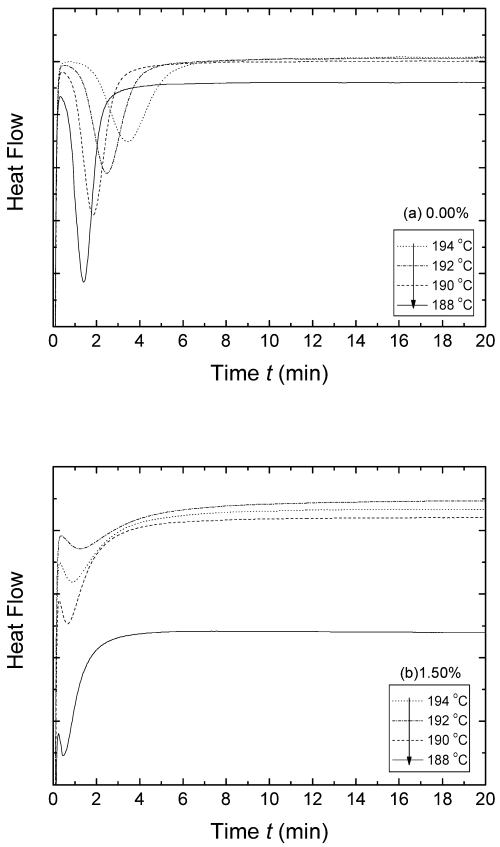

Fig. 1. Heat flow as a function of time during isothermal crystallization a different crystallization temperature by DSC for neat nylon 6 (a), and nylon 6/FG nanocomposite with a FG volume content of 1.5% (b).

From Fig. 1b, one can also read that at all the crystallization temperatures adopted, a significant portion of nylon 6 crystallizes before timing begins. This implies that the temperature at which the crystallization of the nylon 6 in the nanocomposite starts is higher than that of the pure one. This phenomenon is consistent with the DSC analyses presented in [9] for the nylon 6 nanocomposites with various foliated graphite contents but at identical non-isothermal scan rates.

The isothermal crystallization kinetics of a material can be analyzed by evaluating its degree of crystalline conversion as a function of time at a constant temperature. The relative crystallinity at different crystallization time, $X(t)$, can be obtained from the ratio of the area of the exotherm up to time t divided by the total exotherm with an equation given as

$$X(t) = \frac{Q_t}{Q_\infty} = \frac{\int_0^t (\mathrm{d}H/\mathrm{d}t)\mathrm{d}t}{\int_0^\infty (\mathrm{d}H/\mathrm{d}t)\mathrm{d}t}, \quad (1)$$

where Q_t and Q_∞ are the heat generated at time t and infinite time, respectively, and $\mathrm{d}H/\mathrm{d}t$ is the heat flow rate. The development of the relative crystallinity with time for the neat nylon 6 and the nanocomposite samples are plotted in Fig. 2. As can be seen, all the isotherms exhibit a sigmoid dependence with time. The characteristic isotherms are shifted to right along the time axis with increase of crystallization temperature, indicating progressively slower crystallization rate. A slow increase of crystallinity with time after most of the crystallization had taken place is observed and this was attributed to the presence to secondary crystallization [16]. It should be noted that this phenomenon is less significant in the case of the nanocomposite sample.

By assuming that the relative crystallinity increases as the increase of time, analysis of the time-dependent relative crystallinity function $X(t)$ is usually carried out in the context of the Avrami equation [16,17], which can be expressed as

$$X(t) = 1 - \exp(-Kt^n), \quad (2)$$

where K is the Avrami rate constant containing the nucleation and the growth parameters, n is the Avrami exponent whose value depends on the mechanism of nucleation and on the form of crystal growth, and t the crystallization time. It should be noted that based on the original assumptions of the theory, the value of the Avrami exponent n should be an integer, ranging from 1 to 4. Take its double logarithmic form, Eq. (2) can be rearranged as

$$\log[-\ln(1 - X(t))] = \log K + n \log t. \quad (3)$$

From this expression one can expect that if the Avrami approach is valid the plot of $\log[-\ln(1 - X(t))]$ versus $\log t$ should be a straight line for which the slope is equal to n and the intercept is $\log K$.

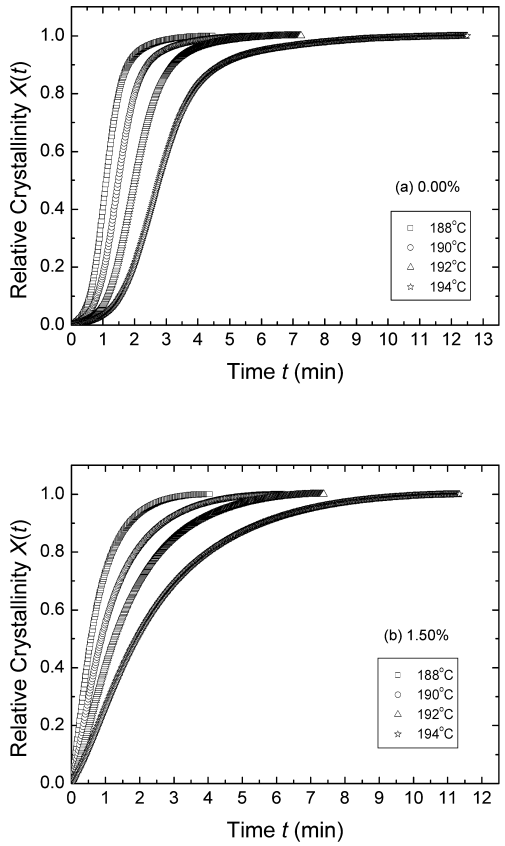

Fig. 2. Relative crystallinity versus crystallization time for various crystallization temperatures from DSC thermograms of (a) neat nylon 6 and (b) nylon 6/FG nanocomposite sample with a FG weight content of 1.50%.

Plots of $\log[-\ln(1 - X(t))]$ vs. $\log t$ for the nylon 6 samples are shown in Fig. 3. It is seen that each curve for the neat nylon 6 in Fig. 3a is composed of three linear sections. The Avrami exponent changed progressively from 1.3 to 3.0 during the initial development of crystallinity, but remained at about 3.2 over the range 10–75% of the crystallization process. Beyond 75%, the exponent lowered to about 1.3 again, indicating a transition of mechanism of crystallization occurred at the point with a relative crystallinity of about 75%. The straight lines in Fig. 3a derived from the fit of the linear portion with a relative crystallinity ranged from 10 to 75% to the Avrami equation (Eq. (3)).

Unlike the neat nylon 6 resin and most semicrystalline polymers, no obvious roll-off at longer times is observed in for nylon/FG nanocomposite sample (see Fig. 3b), implying that the secondary crystallization of nylon 6 in the nanocomposite does not occur under the experimental conditions. This fact demonstrates that the crystallization behavior of nylon 6 in the nanocomposite is different from that of neat nylon 6. For comparison, the regime of about 10–75% conversion in the curves for the nanocomposite

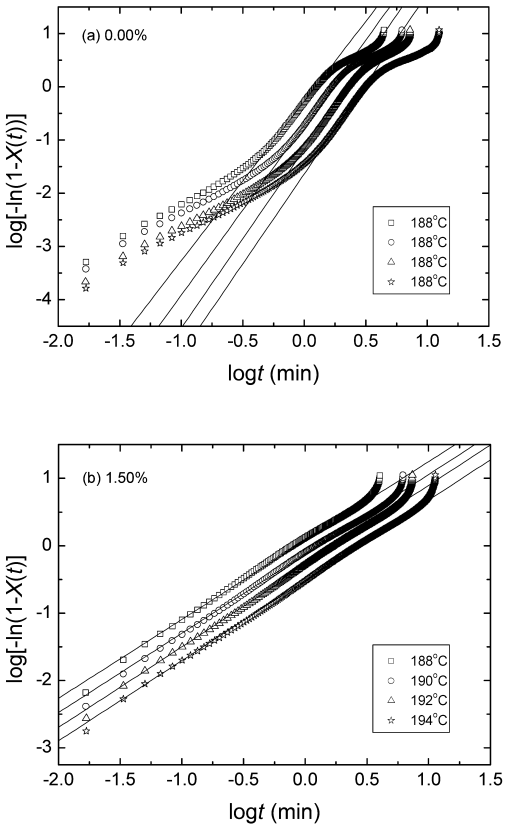

Fig. 3. Plots of $\log[-\ln(1 - X(t))]$ vs. $\log t$ for (a) neat nylon 6 and (b) nylon 6/FG nanocomposite samples isothermally crystallized at the indicated temperature.

Table 1
Parameters of the isothermal crystallization

T_c (°C)	188	190	192	194
0.00%				
n	3.00	3.20	3.36	3.38
K $(\min^{-1/n})^a$	0.5385	0.1912	0.0673	0.0231
K $(\min^{-1/n})^b$	0.5451	0.1948	0.0684	0.0234
$t_{1/2}$ $(\min)^a$	1.0834	1.4875	1.9908	2.7261
$t_{1/2}$ $(\min)^b$	1.0878	1.4964	2.0005	2.7355
$\tau_{1/2}$ $(\min^{-1})^a$	0.9230	0.6723	0.5023	0.3668
$\tau_{1/2}$ $(\min^{-1})^b$	0.9193	0.6683	0.4999	0.3656
t_{max} $(\min)^c$	1.0737	1.4923	2.0086	2.7482
t_{max} $(\min)^d$	1.0694	1.4834	1.9989	2.7388
t_c (min)	4.33	5.33	6.38	9.13
ΔH (J/g)	52.37	52.30	52.25	51.47
1.50%				
n	1.17	1.18	1.20	1.19
K $(\min^{-1/n})^a$	1.1981	0.7596	0.5005	0.3074
K $(\min^{-1/n})^b$	1.2867	0.8122	0.5259	0.3224
$t_{1/2}$ $(\min)^a$	0.5896	0.8741	1.2593	1.9020
$t_{1/2}$ $(\min)^b$	0.6266	0.9252	1.3124	1.9798
$\tau_{1/2}$ $(\min^{-1})^a$	1.6961	1.1440	0.7941	0.5258
$\tau_{1/2}$ $(\min^{-1})^b$	1.5958	1.0809	0.7619	0.5051
t_{max} $(\min)^c$	0.1656	0.2534	0.3962	0.5779
t_{max} $(\min)^d$	0.1559	0.2394	0.3801	0.5552
t_c (min)	4.71	6.06	7.54	11.33
ΔH (J/g)	29.04	34.00	32.93	31.22

[a] Determined from Fig. 2.
[b] Calculated from Eq. (5).
[c] Determined from Fig. 1.
[d] Calculated from Eq. (7).

sample is chosen to determine the exponent n and K according to Eq. (3) and the results are presented in Table 1.

The results indicate that the growth of crystals in nylon 6/FG nanocomposite melt is probably 1D, and the nucleation process is heterogeneous and simultaneous under the experimental conditions [18]. In addition, it is of great interest to compare the Avrami exponent n of nylon 6 in the nanocomposite with that of the neat nylon 6. The values of exponent n for the neat nylon 6 corresponding to the primary crystallization stage are close to 3.0, which mean that the nylon 6 chains tend to take the 3D growth mechanism. However, with the addition of the foliated graphite the mechanism of nucleation and the growth of polyamide crystallite are greatly influenced, leading to the decrease of the Avrami exponent n in the nanocomposite.

3.1.2. Parameters of the isothermal crystallization

Another important parameter is the half-time of crystallization, $t_{1/2}$, which is defined as the time at which the extent of crystallization is 50%. It can be conveniently extracted from the plots of relative crystallinity $X(t)$ versus time t in Fig. 2. The relation between the half-time and the crystallization parameter K can be expressed as

$$K = \ln 2/t_{1/2}^n \quad (5)$$

with n the Avrami exponent. Using Eq. (5) the theoretical values of K and $t_{1/2}$ can be calculated if take one of them from the experimental data. The values of the half-time $t_{1/2}$ and the crystallization parameter K derived both from experimental data and Eq. (5) are listed in Table 1. As can be seen, the values of $t_{1/2}$ and K derived from Eq. (5) agree well with those obtained from the experimental plots.

Usually, $t_{1/2}$ or the reciprocal of $t_{1/2}$, $\tau_{1/2}$, is directly employed to describe the rate of crystallization, G. That is to say $G = (t_{1/2})^{-1} = \tau_{1/2}$. The greater the value of $t_{1/2}$, the lower the rate of the crystallization. The values of $t_{1/2}$ and $\tau_{1/2}$ listed in Table 1 indicate that the nanocomposite sample has a greater rate of crystallization than the neat nylon 6 in the primary stage. The growth rate of crystallization, G, as a function of the crystallization temperature, T_c, is also reported in Fig. 4 for the pure nylon 6 and the nylon 6/FG nanocomposite sample. For both of the two samples the half-time increases with T_c, in agreement with the kinetics theory of crystallization, that expects for crystallization close to the melting temperature, a decrease of G reducing the undercooling [19].

The temperature dependence of the linear growth rate of the spherulites may be derived from the Lauritzen–Hoffman theory for secondary nucleation [20]. Assuming a coherent secondary surface nucleation, the general expression for the

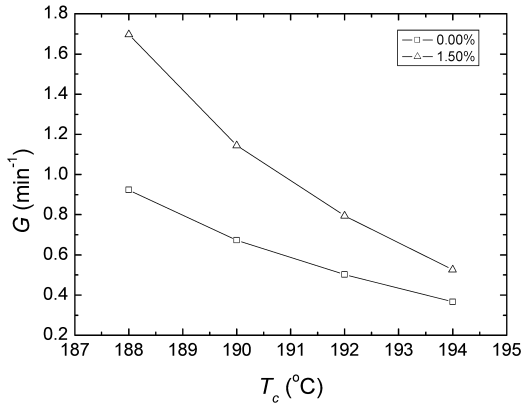

Fig. 4. The rate of crystallization, G versus T_c of isothermal crystallization for the neat nylon 6 and the nanocomposite.

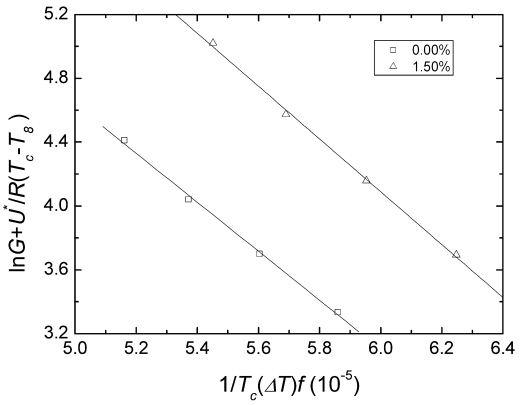

Fig. 5. Plots of $\ln G + U^*/R(T_c - T_\infty)$ versus $1/T_c(\Delta T)f$ for the neat nylon 6 and the nanocomposite.

linear growth rate is given by

$$G = G_0 \exp\left(-\frac{U^*}{R(T_c - T_\infty)}\right)\exp\left(-\frac{K_g}{T_c(\Delta T)f}\right), \tag{6a}$$

where G_0 is a preexponential factor, U^* is the energy for the transport of the macromolecules in the melt and is commonly given by a universal value of 6280 J/mol, T_∞ is a hypothetical temperature below which all the motions associated with the viscous flow ceases, defined as $(T_g - C)$ where T_g is the glass transition temperature and C is a constant equal to 30, R is the universal gas constant, K_g is a nucleation parameter related to the fold and lateral surface energies, ΔT is the undercooling defined as $T_m^0 - T_c$, T_m^0 is the equilibrium melting temperature, f is a corrective factor for the decrease of the enthalpy of fusion with the crystallization temperature, $f = 2T_c(T_c + T_m^0)$. Eq. (6a) is often rearranged as

$$\ln G + \frac{U^*}{R(T_c - T_\infty)} = \ln G_0 - \frac{K_g}{T_c(\Delta T)f}. \tag{6b}$$

Thus, drawing a straight line of the left-hand side of Eq. (6b) against $1/T_c(\Delta T)f$ will give a slope of $-K_g$. Using the obtained values of T_m^0 in the present case (see Section 3.3.1.2) and $T_g = 323$ K for nylon 6, Eq. (6b) is represented in Fig. 5, and the values of the nucleation parameter K_g are derived from the slopes as 1.53×10^5 K^2 and 1.65×10^5 K^2 for the neat nylon 6 and the nanocomposite samples, respectively. It is clear that the nanocomposite sample has a greater K_g, indicating that the motion of the nylon 6 chains is more difficult in the nanocomposite.

Additionally, the time to reach the maximum rate of crystallization t_{max} and the time to crystallize fully t_c can also be used to characterize the rate of crystallization. The data of t_{max} and t_c can be easily find from the isotherms in Fig. 1, and their values for various crystallization temperature are all tabulated in Table 1. Since t_{max} corresponds to the point at which $dQ(t)/dt = 0$, $Q(t)$ is the rate of heat evolution, thus

$$t_{max} = [(n-1)/nK]^{1/n}. \tag{7}$$

The value of t_{max} then can be derived from the Avrami exponent n and the parameter K obtained from the plots of $\log[-\ln(1 - X(t))]$ vs. $\log t$. Both the calculated and the extracted values of t_{max} are listed in Table 1. It is clear that the values of most of the crystallization parameters calculated using the theoretical equations are in good agreement with those obtained from the experimental plots, suggesting that the Avrami analysis works very well in describing the crystallization of nylon 6 from the melt of neat nylon 6 resin and the nanocomposite.

In investigating the dependence of the spherulitic growth rate upon the crystallization temperature, Lin [21] derived the following relation

$$\ln t_{max} = A - \frac{B}{T_c^2 \Delta T}, \tag{8}$$

where A and B are constants, the other variables are the same as defined previously. The possibility that nylon 6 could be described by Avrami equation at the primary stage of the isothermal crystallization can then be tested by simply plotting $\ln t_{max}$ vs. $1/(T_c^2\Delta T)$. Such a linear dependence is,

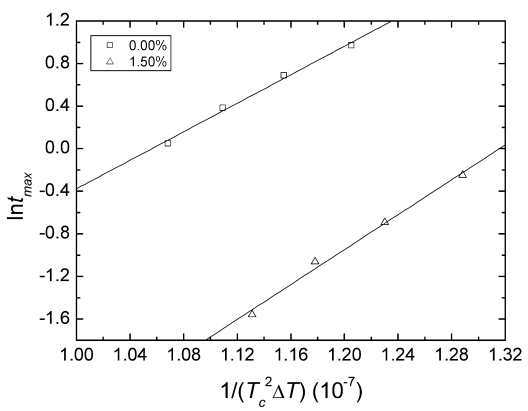

Fig. 6. Plots of $\ln t_{max}$, versus $1/(T_c^2\Delta T)$.

indeed, observed in the present case (Fig. 6), indicating that nylon 6 macromolecules undergo primary crystallization at t_{max} in both the neat nylon 6 and the nanocomposite samples.

3.1.3. Crystallization activation energy

The crystallization process for bulk nylon 6 is assumed to be thermally activated, thus the Avrami parameter K can be used to determine the energy for crystallization. The crystallization rate parameter K can be approximately described by the Arrhenius equation such that [22]

$$K^{1/n} = k_0 \exp(-\Delta E/RT_c) \tag{9}$$

or

$$(1/n)\ln K = \ln k_0 - \Delta E/RT_c,$$

where k_0 is a temperature independent pre-exponential factor, ΔE is an activation energy, R is the gas constant, and T_c the crystallization temperature.

From a graphic representation (Fig. 7) of the experimental data of $\ln K$ against $1/T_c$, ΔE can be determined by the slope of the linear plot. The values of the crystallization activation energy are found to be -271.12 and -354.88 kJ/mol for the neat nylon 6 and the nanocomposite, respectively. Since transforming the molten fluid into the crystalline state involves the release of energy, a greater magnitude of ΔE ($|\Delta E|$) means that the transformation need to release more energy. These results are in consistent with those obtained for the nucleation parameter K_g.

3.2. Non-isothermal crystallization analysis

Although most of the research work was devoted to the crystallization of polymers under isothermal conditions, it is of increasing technological importance to investigate the behavior of thermoplastic semicrystalline polymers during non-isothermal crystallization from the melt, since these conditions are the closet to real industrial processing conditions, i.e. actual processing of polymers is more likely to involve a rate dependent crystallization.

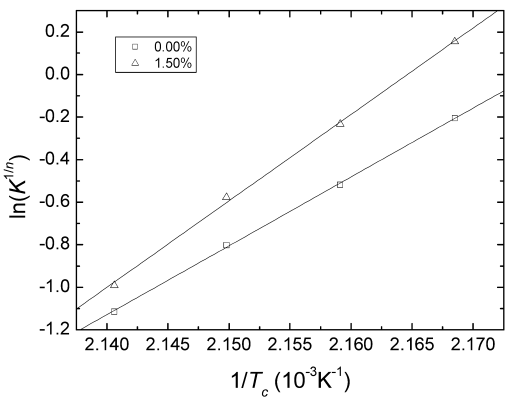

Fig. 7. Plots of $(1/n)\ln K$ against $1/T_c$ of the neat nylon 6 and the nanocomposite sample.

The non-isothermal crystallization exothermal curves of the neat nylon 6 and the nylon 6/FG nanocomposite with an FG content of 1.50 wt% are illustrated in Fig. 8. In both cases, the peak temperature, T_p, which corresponds to the maximum crystallization rate, shifts to lower temperature with increasing cooling rate. It is also seen that the lower the cooling rate, the earlier the crystallization starts.

Similarly, integration of the exothermal peaks during the non-isothermal scan can give the relative crystallinity as a function of temperature or time. In the non-isothermal crystallization, the time t has the relation with the temperature T as follows:

$$t = \frac{|T_0 - T|}{\phi}, \tag{10}$$

where T is the temperature at time t, T_0 is the temperature the crystallization begins ($t = 0$), and ϕ is the cooling rate.

Fig. 9 presents the amorphous fraction of as a function of temperature for nylon 6 and nylon 6/FG nanocomposite. According to Eq. (10), the value to T on X-axis in Fig. 9 can be transformed into crystallization time t as shown in Fig. 10. The lower the cooling rate, the larger the temperature (time) range at which the crystallization occurs, therefore, the transformation is controlled by nucleation. Additionally, all curves have approximately the same S (or reversed S)

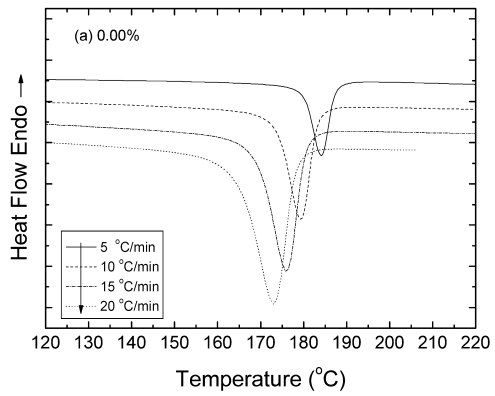

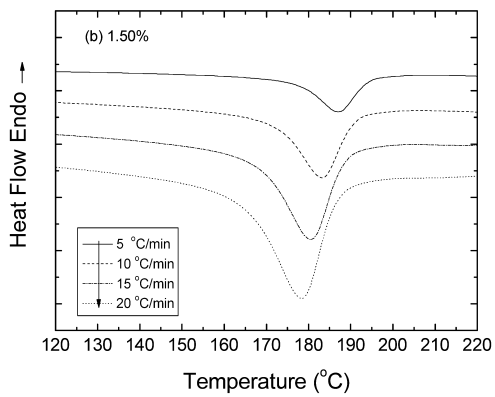

Fig. 8. Heat flow as a function of temperature during non-isothermal crystallization at different cooling rates by DSC for (a) neat nylon 6 and (b) nylon 6/FG nanocomposite with a FG volume content of 1.50%.

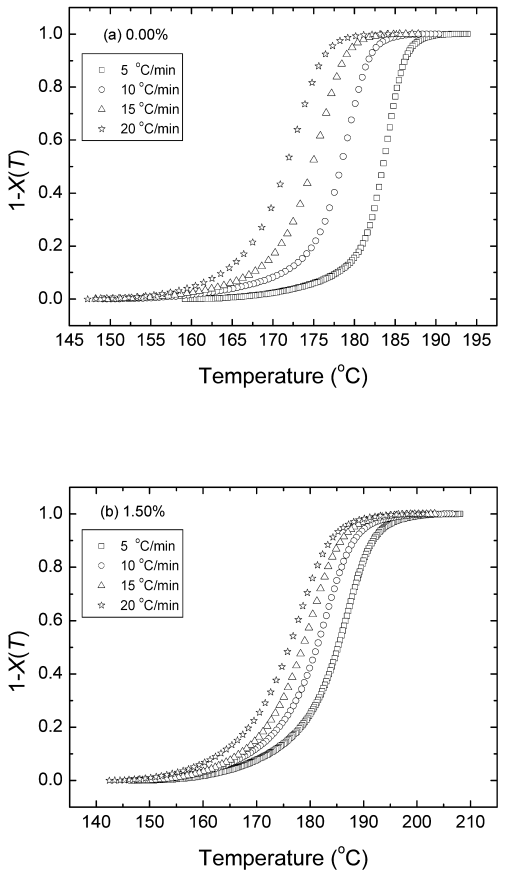

Fig. 9. Plots of amorphous fraction as a function of temperature for (a) nylon 6 and (b) nylon 6/Fg nanocomposite crystallized non-isothermally at various cooling rates.

shape, indicating that only the retardation effect of cooling rate on the crystallization is observed in these curves [23]. Due possibly to the spherulite impingement in the later stage, the curves tend to flat. The values of the peak temperature T_p and the crystallization half-time $t_{1/2}$ collected from the experimental curves of the two samples at various cooling rates are listed in Table 2. It can be seen

Table 2
Values of T_0, T_p, $t_{1/2}$, D, and ΔH at various cooling rates for nylon 6 and its nanocomposite

ϕ (°C/min)	5	10	15	20
0.00%				
T_0 (°C)	193.89	190.41	187.82	185.16
T_p (°C)	184.13	179.38	176.05	173.10
D (°C)	34.69	39.69	39.95	41.57
ΔH (J/g)	49.57	49.12	48.36	46.80
$t_{1/2}$ (min)	2.15	1.26	0.91	0.72
1.50%				
T_0 (°C)	208.11	206.63	203.31	201.16
T_p (°C)	187.08	183.08	180.61	178.33
D (°C)	53.53	58.04	59.01	59.72
ΔH (J/g)	47.83	46.96	46.63	45.72
$t_{1/2}$ (min)	4.59	2.55	1.66	1.27

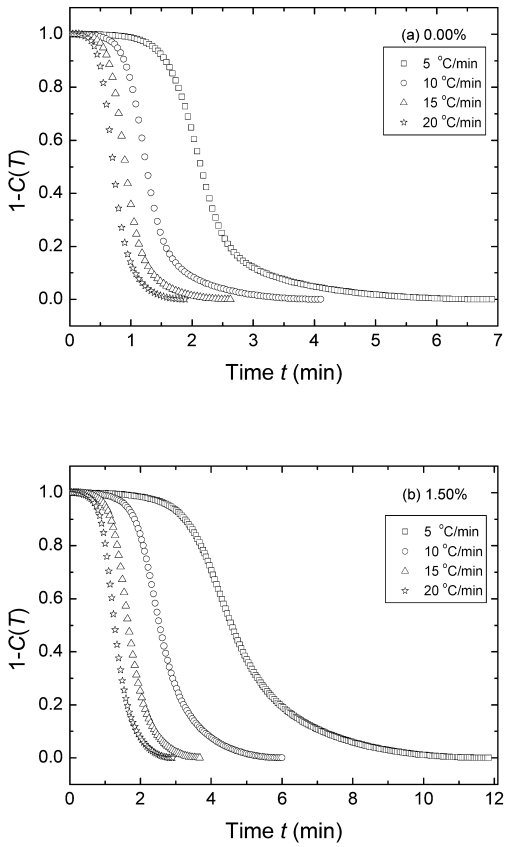

Fig. 10. Plots of amorphous fraction as a function of time for the two nylon 6 samples.

that the values of the peak temperature for nylon 6/FG nanocomposite are higher than those of the neat nylon 6, while the values of the half-time and crystallization time range D of the nanocomposite are also larger than those of the neat nylon 6.

3.2.1. Modified Avrami equation

Based on the assumption that the crystallization temperature is constant, the Avrami equation can be directly used to describe the primary stage of non-isothermal crystallization. In this case, the Avrami equation is expressed as

$$1 - X(t) = \exp(Z_t t^n) \tag{11}$$

or

$$\log[\ln(1 - X(t))] = \log Z_t + n \log t,$$

where Z_t is the rate constant in the non-isothermal crystallization process. Considering the non-isothermal character of the process investigated, the value of Z_t determined from Eq. (11) should be inadequate, due to the influence of the cooling rate. Assuming that the cooling rate is constant or approximately constant, the final form of the parameter characterizing the kinetics of non-isothermal crystallization

is given as follows [24]:

$$\log Z_c = \frac{\log Z_t}{\phi}. \quad (12)$$

Drawing the straight line given by Eq. (11) enable one to obtain the Avrami exponent n and the rate parameter Z_t or Z_c from the slope and the intercept, respectively.

Fig. 11 presents plots of $\log[-\ln(1 - X(t))]$ versus $\log t$ for the neat nylon 6 and the nanocomposite, respectively. Similar to the case of isothermal crystallization, all curves can be divided into three sections. Although the linearity is poor, the modified Avrami equation can be used to describe a large range of relative crystallinity. The linear line in the middle portion of the curves in Fig. 11 is adopted to determine the Avrami exponent n and the corresponding rate parameters.

The derived parameters are listed in Table 3. It is seen that n values of the neat nylon 6 vary from 4.51 to 5.81, and those of the nylon 6/FG nanocomposite range from 4.92 to 5.76, which means the addition of the foliated graphite influences the mechanism of nucleation and the growth of nylon 6 crystallites. It should be noted that all the n values found are higher than 4, implying very complicated crystallization mechanisms in the two samples. The larger the rate parameter Z_c value, the higher the crystallization rate is. At the same cooling rate, the much higher Z_c and $t_{1/2}$

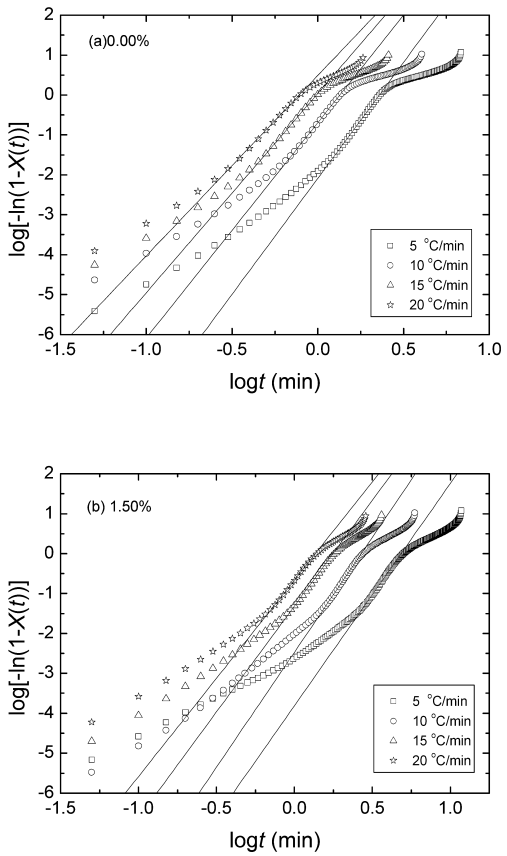

Fig. 11. Plots of $\log[-\ln(1 - X(t))]$ versus $\log t$ for neat nylon 6 (a) and nylon 6/FG nanocomposite (b).

Table 3
Values of n, Z_t and Z_c from the modified Avrami equation at various cooling rates

ϕ (°C/min)	5	10	15	20
0.00%				
n	5.81	5.39	4.99	4.51
Z_t	7.982e-3	0.1975	1.0661	3.0234
Z_c	0.3806	0.8503	1.0043	1.0569
1.50%				
n	5.56	5.75	5.30	4.92
Z_t	1.509e-4	3.299e-3	0.0474	0.2122
Z_c	0.1721	0.5647	0.8160	0.9254

of nylon 6/FG nanocomposite than those of the neat nylon 6 indicate that the graphite nanosheets might hinder the crystallization under non-isothermal conductions. However, as mentioned before, addition of foliated graphite nanosheets increases both the onset and the peak temperatures. This further complicates the problem.

3.2.2. Ozawa model

Considering the effect of cooling rate on the non-isothermal crystallization, Ozawa [25] extended the Avrami theory from isothermal crystallization to the non-isothermal case by assuming that crystallization occurs at a constant cooling rate. According to Ozawa theory, the relative crystallinity, $C(T)$, at temperature T, can be calculated as:

$$C(T) = 1 - \exp[-\kappa_c/\phi^m], \quad (13)$$

where κ_c is the cooling function related to the all over crystallization rate and m is the Ozawa exponent that depends on the dimension of crystal growth. Similarly, Eq. (13) can be changed to its linear form:

$$\log[-\ln(1 - C(T))] = \log \kappa_c - m \log \phi. \quad (14)$$

If this model correctly describes the non-isothermal crystallization kinetics of the nylon 6 samples, then a graphic representation of $\log[-\ln(1 - C(T))]$ as a function of $\log \phi$ will generate a straight line, from which the Ozawa exponent and the kinetic parameter κ_c can be calculated.

Fig. 12 illustrates the plots of $\log[-\ln(1 - C(T))]$ as a function of $\log \phi$. Clearly no straight lines are obtained, indicating the failure of the Ozawa model to provide an adequate description of crystallization in both the neat nylon 6 and the nanocomposite. Because non-isothermal crystallization is a dynamic process in which the crystallization rate is no longer constant but a function of time and cooling rate, the quasi-isothermal treatment of the Ozawa model might be questionable. In the Ozawa analysis, comparison is to be carried out on experimental data representing widely varying physical states of the system, however, these differences have not been taken into account in the model. For instance, in Fig. 9a, the data at 178 °C for the cooling rate of −5 °C/min is at the very latest stage of crystallization,

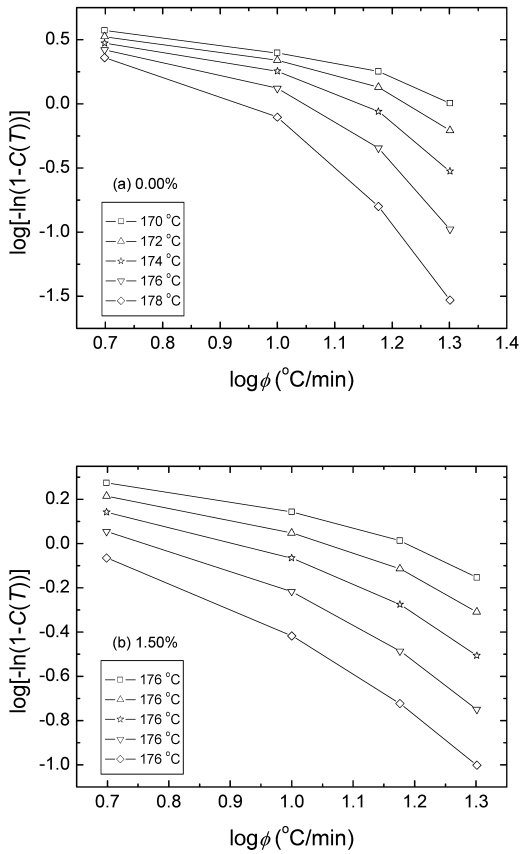

Fig. 12. Ozawa plots of $\log[\ln(1-C(T))]$ vs. $\log\phi$ at indicated temperatures for the two samples.

and for the cooling rate −20 °C/min corresponding to the point when the crystallization just begins. Thus, if the cooling rates vary in a large range and large amount of crystallization occurs as a result of secondary processes, Ozawa model would be not adequate in describing non-isothermal crystallization behaviors. Moreover, effects such as transcrystallization are not considered in the Ozawa theory. It so happens that this particular phenomenon accelerates the average kinetics of transformation, and tends to make up for the volume restriction effects which, on the contrary, slow down crystallization kinetics. As a result, the Avrami exponent n (Ozawa exponent m in this case), has no physical significance any more when strong surface nucleation occurs, because its evolution involves factors with contradictory effects. Therefore, the way it varies when fibers or nucleating agents are added to the bulk polymer become problematic and not easily interpretable [26]. In the present case, the foliated graphite nanosheets act as an additional phase the nylon 6 matrix, making the problem more complicated, thus it is plausible that the applicability of the Ozawa approach fails.

3.2.3. Modified Ozawa equation

On the basis of the findings on the crystallization behavior of PET and PP, Chuah et al. [27] proposed:

$$\ln \kappa_c = \lambda(T - T_1), \tag{15}$$

where λ and T_1 are empirical constants. If the extreme point of the pertinent $\partial C(T)/\partial T$ curve occurs at $T = T_\phi$, i.e.

$$(\partial^2 C(T)/\partial T^2)_{T_\phi} = 0,$$

one has

$$\kappa_c(T_\phi) = \phi^m. \tag{16}$$

Combining Eqs. (13), (15) and (16) leads to

$$\ln[-\ln(1 - C(T))] = \lambda(T - T_\phi). \tag{17}$$

Hence, a linear plot of $\ln[-\ln(1 - C(T))]$ against T would result in the constant λ and the product $-\lambda T_\phi$ from the slope and intercept, respectively. At $T = T_\phi$, Eqs. (15) and (16) lead to

$$T_\phi = m \ln \phi/\lambda + T_1. \tag{18}$$

Thus, the Ozawa exponent m is obtainable from the linear plot of T_ϕ against $\ln \phi/\lambda$.

According to the Ozawa theory, Eq. (17) is valid only for the crystallization regime I [25]. Thus, only the range of the relative crystallinity $C(T)$ of about 0.01–0.40 is used in the foregoing linear regression analyses. The experimental data are exhibited in Fig. 13 in the form of $\ln[-\ln(1 - C(T))]$ against T according to Eq. (17). The parameters estimated from the linear regressions are thus used to plot T_ϕ against $\ln \phi/\lambda$ in accordance with Eq. (18). The resulting plots are illustrated in Fig. 14. Here, the values of the exponent m can then be readily obtained from linear regressions of the curves. The values of m found are 3.98 and 1.61 for the neat nylon 6 and the nanocomposite samples, respectively. These results are similar to those found in the isothermal analyses and suggest that non-isothermal crystallization of nylon 6 in the neat nylon 6 and nanocomposite samples seems to proceed via heterogeneous nucleation, while the neat nylon 6 tends to take a mode of 3D spherulitic growth, the macromolecules in the nanocomposite might prefer a crystallization mode of a mixture of 1D, needle-like and 2D, circular growth.

3.2.4. Combined Avrami equation and Ozawa equation

It is evident that in several cases both the Avrami equation and the Ozawa equation are inadequate in analysis of the non-isothermal crystallization of the polymers. Aiming at find a method to describe exactly the non-isothermal crystallization process, Mo et al. [28] proposed a novel kinetics equation by combing Avrami and Ozawa equation. Under a certain crystallinity degree, Eqs. (11) and (13) can be combined together to give

$$\log Z_t + n \log t = \log \kappa_c - m \log \phi \tag{19a}$$

$$\log \phi = (1/m)\log(\kappa_c/Z_t) - (n/m)\log t \tag{19b}$$

$$\log \phi = \log F(T) - a \log t \tag{19c}$$

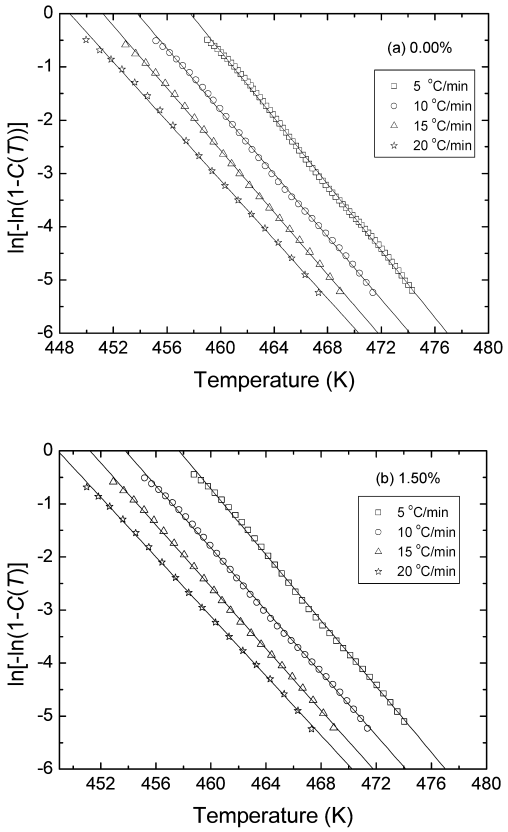

Fig. 13. Plots of $\log[-\ln(1 - C(T))]$ against T for the pure nylon 6 and the nanocomposite samples.

where

$$F(T) = \left[\frac{\kappa_c}{Z_t}\right]^{1/m}, \quad a = n/m.$$

The physical meaning of the rate parameter $F(T)$ refers to the necessary value of cooling rate to reach a defined degree of crystallinity at unit crystallization time. According to Eq. (19c), at a given degree of crystallinity, the plot of $\log \phi$ as a function of $\log t$ gives a straight line with $\log F(T)$ as the intercept and $-a$ as the slope.

Fig. 15 presents plots of $\log \phi$ versus $\log t$ at various degree of crystallinity as indicated. The good linearity of the plots verifies the advantage of the combined approach applied in this case. The values of $F(T)$ and a are listed in Table 4, from which one can read that the values of $F(T)$ increase systematically with increasing relative crystallinity, indicating that at unit crystallization time, a higher cooling rate should be required in order to obtain a higher degree of crystallinity, nevertheless, the values of the parameter a are almost constant.

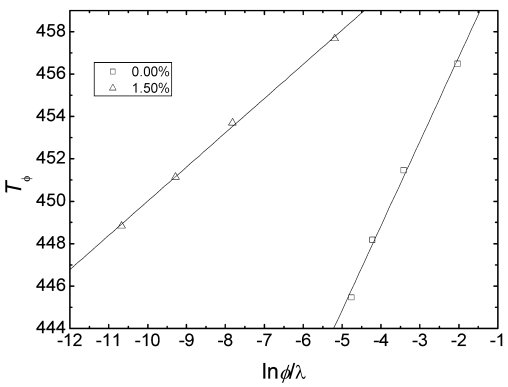

Fig. 14. Plots of T_ϕ against $\ln \phi/\lambda$ for the neat nylon 6 and nylon 6/FG nanocomposite samples.

3.2.5. Crystallization activation energy

By taking into account the influence of various cooling rates ϕ, Kissinger [29] proposed that the activation energy could be determined by calculating the variation of the crystallization peak temperature with the cooling rate. The formula can be given as:

$$\frac{d[\ln(\phi/T_p^2)]}{d(1/T_p)} = -\frac{\Delta E}{R}, \tag{20}$$

where R is the gas constant and T_p is the crystallization peak temperature. The values of $\ln(\phi/T_p^2)$ are plotted as function of $1/T_p$ in Fig. 16 and good linear relations are obtained. From the slopes of the two straight lines generated from linear regression, the values of the activation energy are found to be -213.96 and -289.56 kJ/mol for the neat

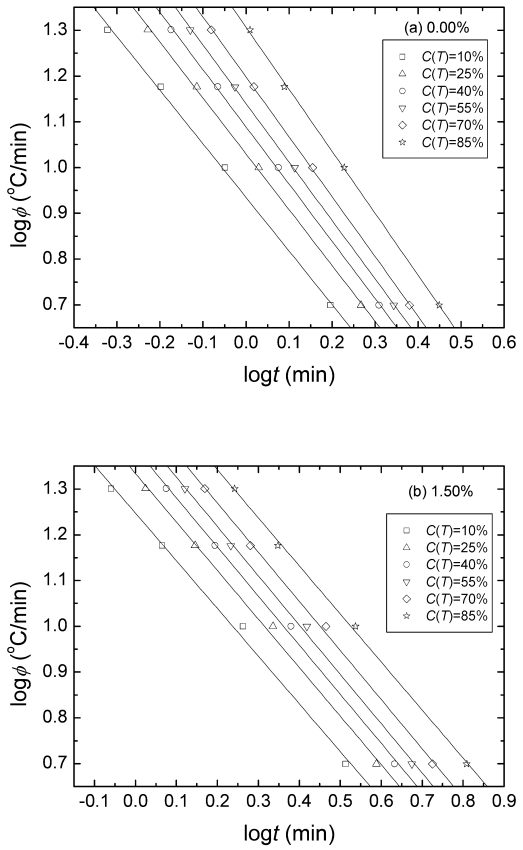

Fig. 15. Plots of $\log \phi$ versus $\log t$ for (a) nylon 6 and (b) nylon 6/FG nanocomposite with a foliated graphite volume content of 1.50% during non-isothermal crystallization.

Table 4
Non-isothermal crystallization kinetics parameters from combination of Avrami–Ozawa equation

	0.00%		1.50%	
	a	*F*(*T*)	*a*	*F*(*T*)
10	1.1708	8.6060	1.0420	17.6767
25	1.2195	10.7152	1.0601	21.5725
40	1.2495	12.2716	1.0727	24.4287
55	1.2771	13.6144	1.0773	27.1394
70	1.3082	15.7834	1.0738	30.4930
85	1.3543	20.2582	1.0501	35.6533

nylon 6 and the nylon 6/FG nanocomposite, respectively. These values are slightly lower than those of the isothermal crystallization process. However, a similar trend is found in this case, that is the magnitude of ΔE is greater for the nanocomposite, suggesting a more difficult motion of the polymer chain segments.

3.3. Melting behaviors

3.3.1. Melting following isothermal crystallization

3.3.1.1. Melting behavior. The DSC heating thermograms of neat nylon 6 and the nylon 6/FG nanocomposite sample are presented in Fig. 17a and b, respectively. It is clear that all the DSC thermograms possess two melting peaks. The first/lower peak shifts more sharply to higher temperatures and is found to start at about 11 °C above the crystallization temperature. However, the last/higher peak changes slightly with increasing crystallization temperature. While up to now, some discrepancies still existed in the origin and mechanism of the presence of multiple thermograms, it is generally believed that different thermal history leads to crystals with different perfection [30]. The cause of the first peaks in the scans thus is assumed to be due to the melting of the smallest lamellae produced by secondary crystallization and in the inter-lamellar layers between the larger crystallites. As such, this growth should not develop until after the primary stage is complete. Since the last peak is less dependent on the crystallization temperature and is much larger that the first one, it might be considered to be originated from the melting of the major crystals formed in the primary crystallization process [12].

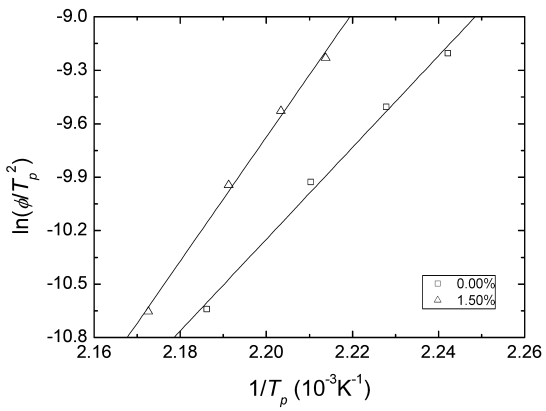

Fig. 16. Kissinger plots for evaluating non-isothermal crystallization activation energy.

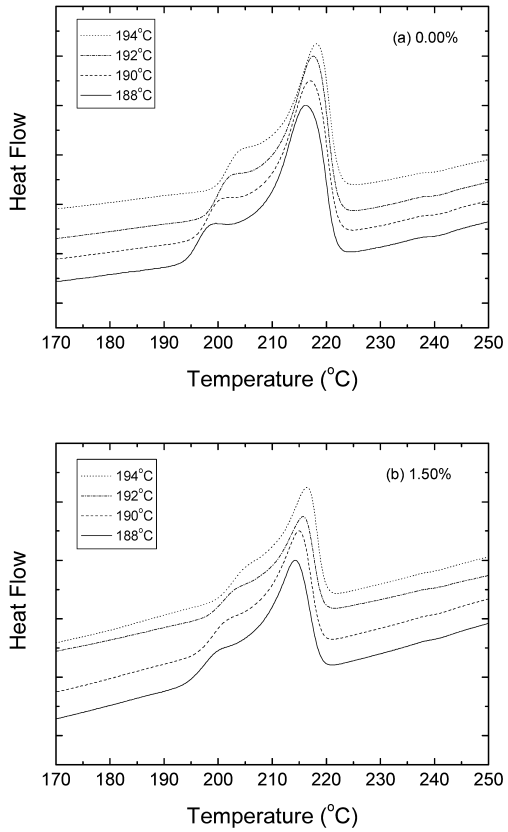

Fig. 17. DSC heating thermograms of neat nylon 6 and the nylon 6/FG nanocomposite samples.

Comparing the thermograms of the neat nylon 6 and the nanocomposite, it is found the first peak is more significant in the neat nylon 6, which indicates there is less secondary crystallization growth taken place during isothermal crystallization. This is in consistent with the results observed in treating the isothermal crystallization kinetics using Avrami theory. In addition, from Table 5 it is seen that both the temperature of the main melting peak and melting enthalpy for the nanocomposite sample are lower than that of the neat nylon 6, suggesting less perfection of the crystals in the nanocomposite sample. This further confirms that presence of foliated graphite nanosheets might hinder the transport of the nylon 6 chains and affect the perfection of their crystals.

3.3.1.2. Equilibrium melting point. For carrying on with quantitative analyses of crystallization behavior, especially to investigate the temperature dependence of the crystallization rates, it is necessary to determine the equilibrium melting point as accurately as possible. The equilibrium melting point is frequently estimated from the melting points from optical microscopy, but it would not generally

Table 5
Values of melting point (T_m) and melting enthalpy (ΔH_f) of the neat nylon 6 and nylon 6/FG nanocomposite melt at a heating rate of 20 °C/min after isothermal crystallization at indicated crystallization temperature T_c

Sample (wt%)	T_c (°C)	T_m (°C)		ΔH_f (J/g)
		Low	High	
0.00	188	199.54	216.00	56.26
	190	200.69	217.02	56.04
	192	202.99	217.64	55.68
	194	204.58	218.20	55.62
1.50	188	200.20	214.26	45.95
	190	201.41	214.97	46.84
	192	203.40	215.82	46.17
	194	204.50	216.43	45.94

be expected to be reliable. Conventionally, experimental melting points from optical microscopy are defined as the temperature where the last trace of birefringence disappears [30]. However, due to the re-crystallization or thickening of the crystalline polymer undergoing heating, the experimentally derived melting points frequently do not reflect the crystals formed at crystallization temperature. Therefore, reliable estimate of the equilibrium melting point should only be made by careful DSC studies. And as a main approach, the procedure suggested by Hoffman and Weeks could be used.

According to Hoffman–Weeks theory [31], the equilibrium melting point may be deduced by plotting the observed apparent melting temperature T_m against the crystallization temperature T_c. The equilibrium melting point is obtained by extrapolation of the resulting straight line to intersect the line $T_m = T_c$. Mathematically, the dependence of T_m on T_c is expressed as

$$T_m = \frac{T_c}{2\beta} + T_m^0\left(1 - \frac{1}{2\beta}\right), \tag{21}$$

where T_m^0 is the equilibrium melting point and β is the lamellar thickening factor which describes the growth of the lamellar thickness during crystallization and is supposed to be always be greater than or equal to 1.

It is well known that the higher the crystallization temperature the more suitable it is to get the equilibrium melting point [32]. As can be seen in Fig. 18, although the lower melting temperatures varies linearly with T_c, the plots are nearly parallel to the line $T_m = T_c$. Therefore, the lines of the last melting temperatures are extrapolated to intersect the line $T_m = T_c$ and give T_m^0 values of 232.0 and 229.6 °C, and β values of 0.722 and 0.736 for the neat nylon 6 and the nylon 6/FG nanocomposite, respectively. The values of T_m^0 are close to that reported in the literature [33], indicating that taking the last melting temperatures as characteristics of the main crystals is reasonable.

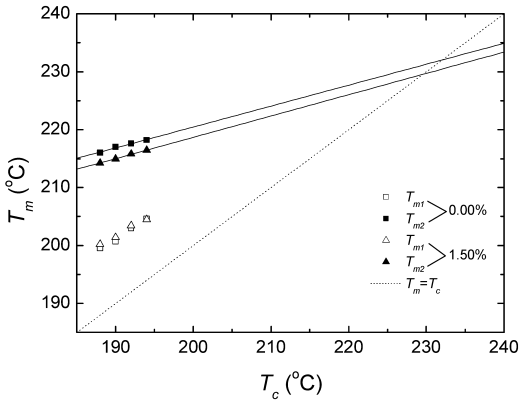

Fig. 18. Melting temperatures as a function of crystallization temperatures for the neat nylon 6 and the nanocomposite samples.

3.3.2. Melting following non-isothermal crystallization

The heating thermograms of the neat nylon 6 and the nylon 6/FG nanocomposite non-isothermally crystallized at different indicated cooling rates are showed in Fig. 19a and b, respectively. It is seen that the thermograms for the neat nylon 6 possess two melting endotherms, while there is only one single peak for the nanocomposite sample. In this case, if the lower peak is also considered to be due to the microcrystallite formed by secondary crystallization and in

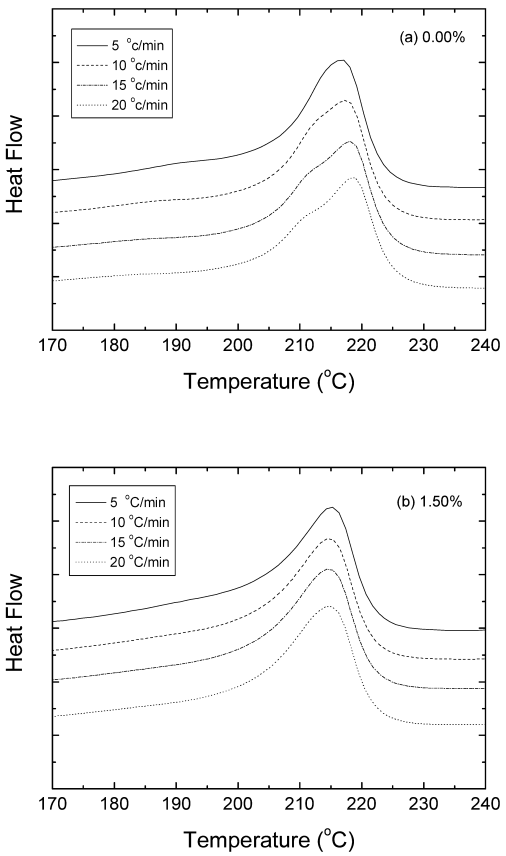

Fig. 19. Melting thermograms of the neat nylon 6 and the nanocomposite sample recorded at a scanning rate of 20 °C/min following non-isothermal crystallization.

the boundary layer between the larger crystallites, it can be drawn that less secondary crystallization occurred in the nanocomposite sample during the non-isothermal crystallization process, similar to the isothermal crystallization case discussed above.

The lower endotherm in Fig. 19a is dependent on the cooling rate, the higher the cooling rate the more apparent the peak. The values melting temperature and enthalpy are collected in Table 6. It is evident that the value of the melting enthalpy decreases with increasing cooling rate for both of the samples. A same trend is observed for the melting temperature of the lower peak of the neat nylon 6. This might be attributed to the fact that under higher supercooling, more molecule chains diffuse into crystalline phase under lower temperature range, at which the motion of the chains reduce, resulting in less perfection of the crystals and lower crystallinity. Additionally, the calculated crystallinity of nylon 6 in the nanocomposite is lower than that of the neat nylon 6, similar to the non-isothermal crystallization process.

4. Conclusion

The investigation of the isothermal and non-isothermal crystallization kinetics of the neat nylon 6 and nylon 6/FG nanocomposite has been carried out by differential scanning calorimetry. The Avrami equation was used to analyze the isothermal crystallization of the two samples. The values of the Avrami exponent n for the neat nylon 6 sample at the primary stage are centered at 3.2, indicating that the process of crystal nucleation and growth is 3D process. However, no obvious roll-off was found in the nanocomposite sample at longer time of crystallization, moreover, the values of the exponent n obtained are about 1.2, much lower than those of the neat nylon 6. This means that the nylon 6 crystallite tends to take a 1D growth mechanism in the nanocomposite under isothermal conditions.

The values of the activation energy derived from the crystallization rate parameter obtained from the Avrami treatment are -269.1 and -337.9 kJ/mol for the neat nylon 6 and the nanocomposite, respectively. And the values of the nucleation parameter K_g obtained are 1.53×10^5 K^2 and 1.65×10^5 K^2 for neat nylon 6 and the nanocomposite, respectively. At each crystallization temperature, the crystallization half-time for the nanocomposite sample are lower than those of the nylon 6, while opposite results were found for the total crystallization time and the crystallization rate parameter.

In the case of the non-isothermal crystallization, the modified Avrami equation and the Ozawa equation were used to analyze the crystallization behaviors of the two samples. However, it was found that the applicability of the two approaches is poor. Using the modified Ozawa equation and a combined Avrami and Ozawa equation the crystallization processes of the two samples could be properly described. Kissinger method was employed to obtain the activation energy of the non-isothermal crystallization processes for the two samples. The activation energy values were found to be -213.96 and -289.56 kJ/mol for the neat nylon 6 and the nanocomposite, respectively. This trend is similar to that found in the isothermal crystallization process. However, the crystallization half-time and total time for the nanocomposite are larger than those of the neat nylon 6, despite that addition of foliated graphite nanosheets increases both the crystallization onset and peak temperatures.

The melting behaviors of the neat nylon 6 and the nylon 6/FG nanocomposite samples were also investigated. The multiple melting peaks were ascribed to different crystal perfection during crystallization processes. Evidences showed that addition of the foliated graphite nanosheets might hinder the motion of the nylon 6 molecule chains, leading to less perfection of the crystals. However, the secondary crystallization was also reduced. The studies on the melting behaviors following the isothermal crystallization focused on the determination of the equilibrium melting point. It was found that the equilibrium melting point is higher for the neat nylon 6 than that in the nanocomposite sample.

Compared with investigations in the literatures [33,34,35], it can be seen that consistent results (i.e. Avrami exponent n and activation energy) could be found for the neat nylon 6 in the present isothermal crystallization study. However, since it has been well demonstrated that polymerization method can greatly influence the properties of nylon 6, different results are expected between our samples and those studied by other researchers. Moreover, owing to the very different surface properties between clay and foliated graphite, the filler-matrix interactions [36] will be very different, despite that FG and clay possesses similar layered structure. On the other hand, based on the above demonstration, it is clear that incorporation of nanoscale foliated graphite significantly influences the crystallization and melting behaviors of the nylon 6. The crystallization process might be a combination of nucleation and

Table 6
Values of melting point (T_m) and melting enthalpy (ΔH_f) of the neat nylon 6 and nylon 6/FG nanocomposite melt at a heating rate of 20 °C/min after non-isothermal crystallization at indicated cooling rates ϕ

Sample (wt%)	ϕ (°C/min)	T_m (°C)		ΔH_f (J/g)
		Low	High	
0.00	5	212.64	217.07	57.73
	10	211.55	217.21	55.23
	15	211.22	218.09	52.18
	20	210.96	218.96	49.69
1.50	5	–	215.30	56.31
	10	–	214.43	53.91
	15	–	214.79	51.04
	20	–	215.16	48.63

crystallization growth. Foliated graphite nanosheets may act as a heterogeneous nucleation for the crystallization of nylon 6, while in the same time their presence hinders the transport of the molecule chains, resulting in a decrease of the crystallization growth rate. However, as is well known, the differences in molecular weight of nylon 6 might also be an important factor. This is under our intensive scrutiny.

Acknowledgements

The authors are grateful to Xinren Lan and Dingcai Wu for doing the DSC measurements. The valuable advises, criticisms and theoretical guidance from Dr Zhiyong Lin are greatly acknowledged. We also enjoy helpful discussions with Dr Hao Qian, Lifeng Cai and Jun Yang. The help of Cuiling Wu, Jianxin Weng and Fengying Xiao are also appreciated. This work was sponsored by National Natural Science Foundation of China (grant 20174012).

References

[1] Pan YX, Yu ZZ, Ou YC, Hu GH. J Polym Sci Part B Polym Phys 2000;38:1626.
[2] Chen GH, Wu DJ, Weng WG, Yan WL. J Appl Polym Sci 2001;82:2506.
[3] Chen GH, Wu DJ, Weng WG, He B, Yan WL. Polym Int 2001;50:980.
[4] Chen GH, Wu DJ, Weng WG, Ye LH, He B, Yan WL. Acta Polym Sin 2001;6:803.
[5] Chen GH, Wu DJ, Weng WG, Yan WL. Polym Engng Sci 2001;41:2148.
[6] Xiao P, Xiao M, Gong K. Polymer 2001;42:4813.
[7] Chen GH, Wu DJ, Weng WG, Wu CL. Carbon 2003;41:579.
[8] Chen GH, Wu CL, Weng WG, Wu DJ, Yan WL. Polymer 2003;44:1781.
[9] Weng WG, Chen GH, Wu DJ, Wu CL. Direct fabrication of nylon 6/foliated graphite electrically conducting nanocomposites via in-situ polymerization upon ultrasonic irradiation, submitted.
[10] Weng WG, Chen GH, Wu DJ, Wu CL. Transport properties of nylon 6/foliated graphite nanocomposites, submitted.
[11] Chen GH, Weng WG, Wu DJ, Wu CL. Nonlinear conduction in the nylon 6/foliated graphite nanocomposites above the percolation threshold, Journal of Polymer Science (B). Polymer Physics. In press.
[12] Lu XF, Hay JN. Polymer 2001;42:9423.
[13] Di Lorenzo ML, Silvestre C. Prog Polym Sci 1999;24:917.
[14] Kojima Y, Matsuoka T, Takahashi H, Kurauchi T. J Appl Polym Sci 1994;51:683.
[15] Mathias LJ, Davis RD, Jarret WL. Macromolecules 1999;32:7958.
[16] Avrami M. J Chem Phys 1940;8:212.
[17] Avrami M. J Chem Phys 1939;7:1103.
[18] Wunderlich BI. Thermal characterization of polymeric materials, 2nd ed. New York: Academic Press; 1997.
[19] Silestre C, Cimmino S, D'Alna E, Di Lorenzo ML, Di Pace E. Polymer 1999;40:519.
[20] Hoffman JD, Davis GT, Lauritzen JI. In: Hanny NB, editor. Treatise on solid state chemistry, vol. 3. New York: Plenum Press; 1976. p. 7.
[21] Lin CC. Polym Engng Sci 1983;23:113.
[22] Cebe P, Hong SD. Polymer 1986;27:183.
[23] Liu X, Wu Q. Eur Polym J 2002;38:1383.
[24] Jeziorny A. Polymer 1978;19:1142.
[25] Ozawa T. Polymer 1971;12:150.
[26] Caze C, Devaux E, Crespy A, Cavrot JP. Polymer 1997;38:497.
[27] Chuah KP, Gan SN, Chee KK. Polymer 1998;40:253.
[28] Liu J, Mo Z. Acta Polym Sin 1993;1:1.
[29] Kissinger HE. J Res Natl Stand 1956;57:217.
[30] Liu T, Mo Z, Wang S, Zhang H. Eur Polym J 1997;33:1405.
[31] Hoffman JD, Weeks JJ. J Res Natl Bur Stand 1962;A73:64.
[32] Wang GM, Yan DY, Bu HS. Chin J Polym Sci 1998;16:2642.
[33] Liu L, Zhu X, Qi Z. Acta Polym Sin 1999;6:274.
[34] Turska E, Gogolewski S. Polymer 1971;12:629.
[35] Fornes TD, Paul DR. Polymer 2003;44:3945.
[36] Wu Q, Liu X, Berglund LA. Polymer 2002;43:2445.